Mathematical Statistical Mechanics

COLIN J. THOMPSON

Princeton University Press
Princeton, New Jersey

To my parents, and to
Michal, Ben, and David

Published by Princeton University Press, Princeton, N.J.
In the U.K.: Princeton University Press, Guildford, Surrey

LCC 77-150071

ISBN 0-691-08219-7 (hardcover edition)
ISBN 0-691-08220-0 (paperback edition)

Originally published 1972 by The Macmillan Company

First Princeton University Press printing, 1979

CHAPTER 7

Some Applications of the Ising Model to Biology

7-1 Introduction

7-2 Myoglobin and Classical Enzymes

7-3 Hemoglobin

7-4 Monod–Wyman–Changeux Model for Hemoglobin and Allosteric Enzymes

7-5 Decorated Ising Models for Allosteric Enzymes

7-6 Ising Models for DNA

PROBLEMS

7-1 Introduction

The Ising and related models have been applied with some success to a number of biological systems. We shall discuss three examples here: hemoglobin, allosteric enzymes, and deoxyribonucleic acid (DNA). These examples are by no means exhaustive, but they illustrate how general lattice combinatoric problems and their methods of solution may be applied to biological problems.

The common feature in the examples we shall consider here is "cooperativity," which is playing a role of increasing importance in biology these days. Hemoglobin, for example, which is the oxygen carrier in red blood cells, has four distinct binding sites for oxygen with apparent interactions between the sites. In other words, if a molecule of oxygen is bound to a hemoglobin molecule, it will be more likely than not to bind other oxygen molecules. This cooperative interaction between the binding sites reflects itself in the saturation curve shown in Figure 7.1, where the percentage of oxygenated hemoglobin is plotted as a function of the partial pressure of oxygen (or equivalently the concentration of oxygen).

It is clear from the S, or sigmoid, shape of the hemoglobin saturation curve that binding of a few molecules of oxygen favors the binding of more and

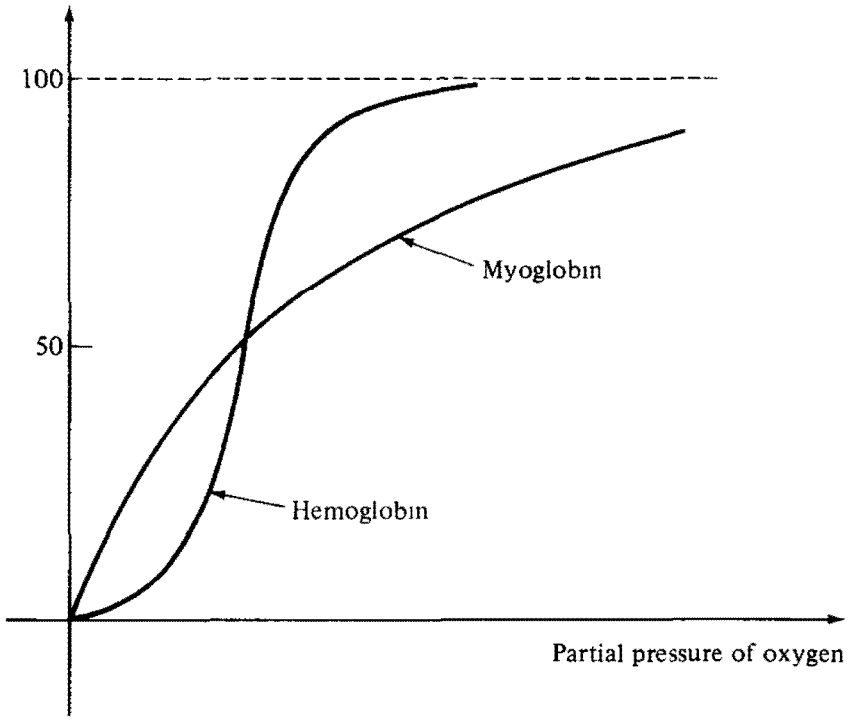

FIGURE 7.1. Percentage of oxygenated hemoglobin and myoblogin as a function of the partial pressure of oxygen.

that binding occurs best at high oxygen concentrations. This naturally makes the hemoglobin molecule a very efficient little machine, since in the lungs where the oxygen concentration is high binding is easy, and, as hemoglobin travels through the body to places with low oxygen concentration, the oxygen leaves the molecule rather easily.

In Figure 7.1 the saturation curve for hemoglobin is compared with the corresponding curve for myoglobin, the oxygen-bearing molecule found in muscle tissue, which has only one binding site for oxygen and hence no chance of displaying any cooperative effects.

A similar situation holds for enzymes, which are catalysts for biochemical reactions. The agent undergoing a particular reaction is usually referred to as the substrate, and the reaction of the substrate, catalyzed by an enzyme, proceeds by substrate molecules occupying distinct binding sites on the enzyme. For a "classical enzyme," the initial reaction rate, which is assumed to be proportional to the number of occupied sites on the enzyme, as a function of substrate concentration, has the same form as the myoglobin saturation curve, showing that there is no apparent interaction between the (possibly many) distinct binding sites. A number of enzymes, the "allosteric enzymes,"

were recently found, however, to have an S-shaped initial reaction-rate curve reflecting some degree of cooperativity among the binding sites.

Finally, DNA also has an S-shaped denaturation or melting curve; i.e., the fraction of broken bonds as a function of temperature has the same form as the hemoglobin saturation curve. If one accepts the Watson–Crick model for DNA, which pictures the molecule as a double helix with hydrogen bonds connecting the two strands, denaturation occurs through the breaking of the hydrogen bonds as the temperature is increased. The denaturation process is then often referred to as the helix-coil transition, and the fraction of broken bonds as a function of temperature gives the "melting curve." The S shape of the melting curves presumably means that the bond-breaking process is cooperative rather than random.

To set the stage for a discussion of the cooperative processes described above we present in the next section a model for the myoglobin and classical enzyme noncooperative processes. In the following sections we shall discuss the structure and function of hemoglobin, allosteric enzymes, and DNA in more detail and show how the random or independent model in Section 7-2 can be modified to take cooperativity into account.

For some background, the interested reader is referred to Perutz (1964) for hemoglobin, Changeux (1965) for enzymes, and Watson (B1968) for DNA.

7-2 Myoglobin and Classical Enzymes

Consider an enzyme with n noninteracting or independent binding sites for substrate ($n = 1$ corresponds to myoglobin and in this case the "substrate" is oxygen). We number the sites by an index $i = 1, 2, \ldots, n$ and associate with each site a parameter μ_i which takes two values, $+1$ if the ith site is occupied by substrate and -1 if the ith site is unoccupied by substrate. (It would perhaps be better to consider lattice gas variables $t_i = 1$ or 0 instead of $\mu_i = +1$ or -1, respectively, but we will see in the following sections that the relation to the Ising model is made easier by starting with the Ising magnet variables $\mu_i = \pm 1$.)

A configuration of the molecule is specified by the values of $\mu_1, \mu_2, \ldots, \mu_n$. In other words, a particular configuration specifies which sites are occupied and which sites are unoccupied. Since there are two states for each site, there are 2^n possible configurations. Henceforth we shall denote a configuration by

$$\{\mu\} = (\mu_1, \mu_2, \ldots, \mu_n). \tag{2.1}$$

The quantity we wish to calculate is the average number of occupied sites on the enzyme. In a *particular configuration* $\{\mu\}$, the number $N\{\mu\}$ of occupied sites is given by

$$N\{\mu\} = \sum_{i=1}^{n} \tfrac{1}{2}(1 + \mu_i) \tag{2.2}$$

since by definition $\frac{1}{2}(1 + \mu_i)$ is 1 when the ith site is occupied and zero when the ith site is unoccupied. The average number of occupied sites N is then defined by

$$N = \sum_{\{\mu\}} N\{\mu\}P\{\mu\}, \tag{2.3}$$

where the sum is over all (2^n) configurations $\mu_1 = \pm 1, \ldots, \mu_n = \pm 1$ and $P\{\mu\}$ is the probability of the configuration $\{\mu\}$.

So far the discussion has been completely general. To proceed further we must specify the probability distribution $P\{\mu\}$. In the case of independent binding sites we define $p(+1)$ to be the probability that a site is occupied and $p(-1)$ to be the probability that a site is unoccupied. Since a site is either occupied or unoccupied we must have

$$p(+1) + p(-1) = 1. \tag{2.4}$$

To simplify the algebra we now define quantities C and J by

$$p(+1) = Ce^{J}, \qquad p(-1) = Ce^{-J}, \tag{2.5}$$

where, from Equation 2.4,

$$C = (2 \cosh J)^{-1}. \tag{2.6}$$

Equation 2.5 can then be written simply as

$$p(\mu_i) = (2 \cosh J)^{-1} \exp(J\mu_i), \tag{2.7}$$

which gives the probability distribution for the ith site.

Now in the case of independent binding sites the probability distribution for the whole molecule $P\{\mu\}$ is simply the product of the probability distributions for each site, i.e.,

$$P\{\mu\} = \prod_{j=1}^{n} p(\mu_j). \tag{2.8}$$

We are now in a position to calculate the average number N of occupied sites. From Equations 2.2, 2.3, 2.7, and 2.8 we have

$$N = \tfrac{1}{2}\sum_{i=1}^{n}\sum_{\{\mu\}}(1+\mu_i)\prod_{j=1}^{n}p(\mu_j), \tag{2.9}$$

and from the normalization condition 2.4,

$$\begin{aligned}\sum_{\{\mu\}}\prod_{j=1}^{n}p(\mu_j) &= \sum_{\mu_1=\pm 1}p(\mu_1)\sum_{\mu_2=\pm 1}p(\mu_2)\cdots\sum_{\mu_n=\pm 1}p(\mu_n)\\ &= 1.\end{aligned} \tag{2.10}$$

Also, after summing over μ_j, $j \neq i$, in Equation 2.9, we obtain

$$\begin{aligned}\sum_{\{\mu\}}\mu_i\prod_{j=1}^{n}p(\mu_j) &= \sum_{\mu_i=\pm 1}\mu_i\,p(\mu_i)\\ &= p(+1)-p(-1)\\ &= \tanh J,\end{aligned} \tag{2.11}$$

where in the last step we have used Equations 2.5 and 2.6. Combining Equations 2.9, 2.10, and 2.11 we then have

$$N = \frac{n}{2}(1+\tanh J). \tag{2.12}$$

Defining α by

$$\alpha = \exp(2J) \tag{2.13}$$

we can write Equation 2.12 in the form

$$f(\alpha) = \frac{N}{n} = \frac{\alpha}{1+\alpha}, \tag{2.14}$$

which is the classical Michaelis–Henri equation for enzyme kinetics if α is interpreted as the concentration of substrate. From Equations 2.5 and 2.13, α is the ratio of the probability that a site is occupied to the probability that a site is unoccupied, so it seems reasonable to interpret α as a measure of the concentration of substrate.

The Michaelis–Henri equation (2.14) fits the myoglobin saturation curve (Figure 7.1) and the initial reaction-rate curve for classical enzymes extremely well. Note that the "units" in Equation 2.14 are chosen so that half-saturation occurs at concentration unity.

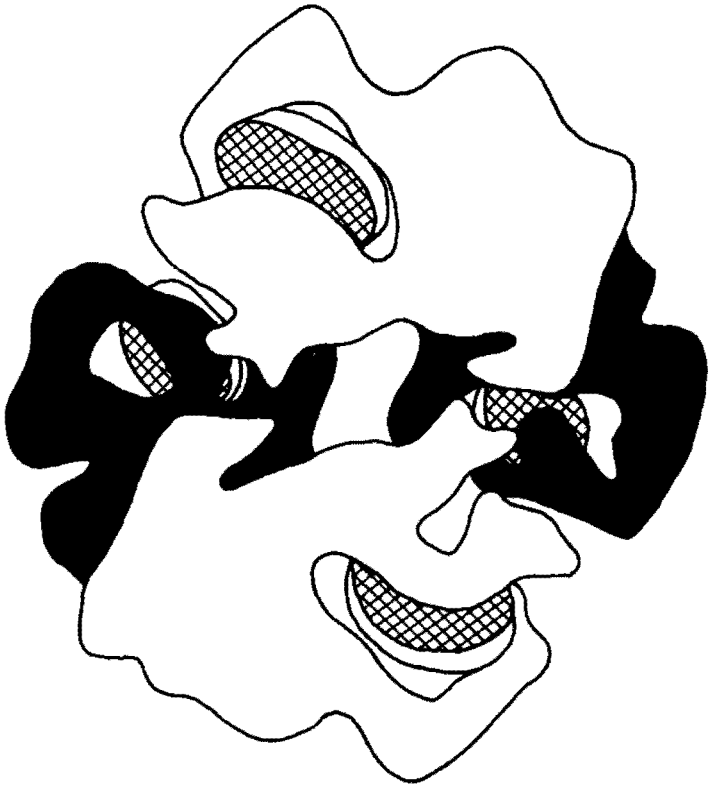

FIGURE 7.2. Schematic illustration of the hemoglobin molecule showing the four hemes (hatched) and the associated α (white) and β (black) amino acid chains.

7-3 Hemoglobin

The hemoglobin molecule is huge, with a molecular weight of about 64,500. It is composed of about 10,000 atoms of hydrogen, carbon, nitrogen, oxygen, sulfur, and four atoms of iron which lie at the center of a group of atoms that form the pigment heme. The heme gives blood its red color, and each heme constitutes a binding site for an oxygen molecule.

The structure of hemoglobin, shown schematically in Figure 7.2, was first unraveled by Perutz et al. (1960) after 23 years or so of painstaking work. Their primary tool was X-ray diffraction, which came into its own in the 1950s as a means for studying the structure of large molecules. Using X-ray diffraction techniques, for example, Kendrew found the structure of myoglobin [see Perutz (1964)] and Wilkins's X-ray pictures of DNA lead to the discovery of the Watson–Crick double-helix model for DNA [see Watson (B1968)]. All these remarkable events occurred in London and Cambridge (England) in the 1950s.

As shown in Figure 7.2, hemoglobin consists of four (hatched) binding sites, or hemes, and, in normal form, two types of amino acid chains, the α and β chains, shown as white and black, respectively, in Figure 7.2. The unlike chains are rather strongly coupled to one another, whereas the like chains have virtually no contacts with one another. To a good approximation the hemes are at the vertices of a regular tetrahedron, shown schematically in Figure 7.3 with the associated amino acid chains. The slight asymmetry of the real molecule reflects itself in the different number of contacts the β chains have with the α chains; in one case 34 residues participate and in the other case 19 residues participate. We shall assume for simplicity that the *degree of cooperativity or interaction* among hemes coupled by different chains is symmetric. (The nonsymmetric case can also be handled with the present formalism.) We shall also assume that interactions among the hemes are transmitted solely through the α-β contacts. In other words, from Figure 7.3, heme 1 interacts with hemes 2 and 4 but not with 3, heme 2 interacts with hemes 1 and 3 but not with 4, and so forth. *This means that we can represent the hemoglobin molecule by a ring of four sites with nearest-neighbor sites only interacting.* To be a little more general, let us consider now a ring of n sites as shown in Figure 7.4. The problem is to calculate the average number of

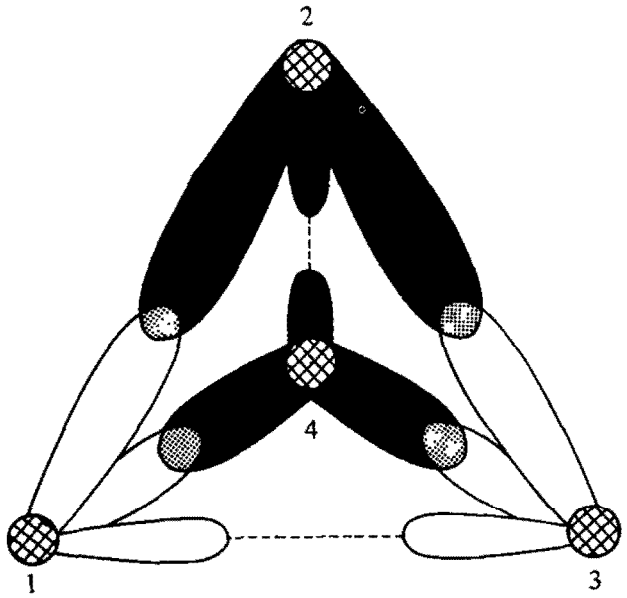

FIGURE 7.3. Simplified model for hemoglobin. The four hemes are approximately situated on the vertices of a regular tetrahedron. Unlike chains are rather strongly coupled, whereas like chains have virtually no contacts with one another.

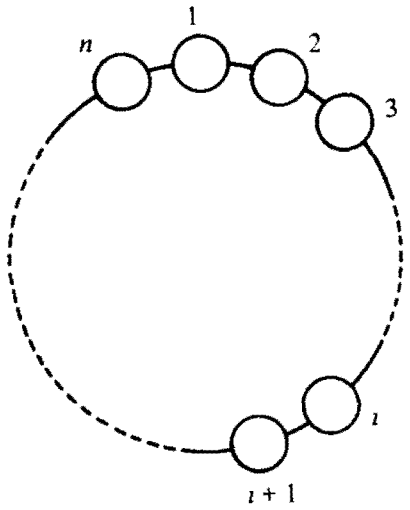

FIGURE 7.4. Nearest-neighbor interaction model for a molecule consisting of n binding sites.

occupied sites defined by Equation 2.3. Assuming that only nearest-neighbor sites interact, we can take the probability distribution $P\{\mu\}$ to be of the form

$$P\{\mu\} = Z^{-1} \prod_{i=1}^{n} \exp(J\mu_i)\exp(U\mu_i\mu_{i+1}), \tag{3.1}$$

where Z is such that $P\{\mu\}$ is properly normalized $\left(\sum_{\{\mu\}} P\{\mu\} = 1\right)$, i.e.,

$$Z = \sum_{\{\mu\}} \prod_{i=1}^{n} \exp(J\mu_i)\exp(U\mu_i\mu_{i+1}) \tag{3.2}$$

and $\mu_{n+1} = \mu_1$. The first factor in the product (Equation 3.1), $\exp(J\mu_i)$, represents the independent binding term (see Equations 2.7 and 2.8) and the second term, $\exp(U\mu_i\mu_{i+1})$, represents interactions or correlations between nearest-neighbor sites, which is attractive when $U > 0$ and repulsive when $U < 0$ (so $U > 0$ for hemoglobin). Z (Equation 3.2) will be recognized immediately as the partition function of a one-dimensional Ising magnet in an external magnetic field kTJ, with nearest-neighbor coupling constant equal to $-kTU$. In magnetic language, N defined by Equations 2.2 and 2.3 is equal to $n(1 + m)/2$, where m is the magnetization per spin.

One point which should be stressed is that $P\{\mu\}$ (*Equation* 3.1) *is the most general probability distribution describing nearest-neighbor correlations.* [Since $\mu_i^2 = 1$ and $(\mu_i\mu_{i+1})^2 = 1$, the most general functions of μ_i and of $\mu_i\mu_{i+1}$ are linear functions, and as was shown in Section 6-1, linear functions of a given product of μ's can always be expressed as exponentials, and vice versa.]

To evaluate the average number of occupied sites N (Equation 2.3), we note first of all from Equations 2.2, 3.1, and 3.2 that

$$\begin{aligned} N &= \sum_{\{\mu\}} \left[\frac{1}{2}\sum_{i=1}^{n}(1+\mu_i)\right] P\{\mu\} \\ &= \frac{n}{2} + \frac{1}{2}\sum_{\{\mu\}}\left(\sum_{i=1}^{n}\mu_i\right) P\{\mu\} \\ &= \frac{n}{2} + \frac{1}{2}\frac{\partial}{\partial J}(\log Z). \end{aligned} \tag{3.3}$$

Now, in Section 5-3 it was shown that

$$Z = \lambda_1^n + \lambda_2^n \qquad \text{(Equation 3.12 of Chapter 5)} \tag{3.4}$$

where λ_1 and λ_2 are the eigenvalues of the transfer matrix (Equation 3.10 of Chapter 5)

$$\mathbf{L} = \begin{pmatrix} \exp(U+J) & \exp(-U) \\ \exp(-U) & \exp(U-J) \end{pmatrix}, \tag{3.5}$$

i.e. (Equation 3.14 of Chapter 5),

$$\left.\begin{matrix}\lambda_1 \\ \lambda_2\end{matrix}\right\} = e^U \cosh J \pm (e^{-2U} + e^{2U}\sinh^2 J)^{1/2}. \tag{3.6}$$

Equations 3.3 and 3.4 then give

$$N = \frac{n}{2}\left[1 + (\lambda_1^n + \lambda_2^n)^{-1}\left(\lambda_1^{n-1}\frac{\partial\lambda_1}{\partial J} + \lambda_2^{n-1}\frac{\partial\lambda_2}{\partial J}\right)\right], \tag{3.7}$$

and it is straightforward, but rather tedious, to show from Equation 3.6 that in terms of the interaction parameter U and the concentration $\alpha = \exp(2J)$ (Equation 2.13) the average fraction of occupied sites is given by

$$\begin{aligned} f(\alpha) &= \frac{N}{n} \\ &= \frac{\alpha\{(1+\alpha+\delta)^{n-1}[1 + (2e^{-4U} + \alpha - 1)/\delta] \\ &\qquad + (1+\alpha-\delta)^{n-1}[1 - (2e^{-4U} + \alpha - 1)/\delta]\}}{(1+\alpha+\delta)^n + (1+\alpha-\delta)^n}, \end{aligned} \tag{3.8}$$

where

$$\delta = [(\alpha-1)^2 + 4\alpha\exp(-4U)]^{1/2}. \tag{3.9}$$

It is to be noted that in the limit $U = 0$, Equation 3.8 reduces to the classical Michaelis–Henri equation (2.14). In the limit $U \to \infty$, $\delta = |\alpha - 1|$, and Equation 3.8 reduces to the Hill equation

$$f(\alpha) = \frac{\alpha^n}{1 + \alpha^n}, \tag{3.10}$$

after Hill, who first attempted to fit hemoglobin saturation curves to this form (the fit is actually reasonably good for $n \approx 2.6$).

For hemoglobin, $n = 4$ and Equation 3.8 takes the simple form

$$f(\alpha) = \frac{\alpha[K + (2K + K^2)\alpha + 3K\alpha^2 + \alpha^3]}{1 + 4K\alpha + (4K + 2K^2)\alpha^2 + 4K\alpha^3 + \alpha^4}, \tag{3.11}$$

where

$$K = \exp(-4U). \tag{3.12}$$

Apart from trivial changes in the scale of concentration, Equation 3.11 is identical with Pauling's model [Pauling (1935)] and is a special case of the square model of Koshland et al. (1966).

In Equation 3.11 there is only one adjustable parameter, K, which is determined by fitting to one experimental point. The resulting theoretical curve for the choice $K = 0.11$ (i.e., from Equation 3.12, $U = 0.55$), is compared with experiment in Figure 7.5. The agreement is reasonably good, but there appears to be a slight systematic deviation from the theoretical curve at high oxygen concentrations. This is probably due to the asymmetric nature of the molecule. As mentioned above, this can be taken into account, specifically in the model, by taking two coupling constants U_1 and U_2 for the two different contacts between unlike chains. With one extra parameter, however, a perfect fit to experiment is almost assured. In fact, a number of two-parameter models, particularly the Monod–Wyman–Changeux model discussed in the following section, give remarkably good results. What is perhaps surprising is the fit obtained using only a one-parameter model.

One interesting feature of hemoglobin saturation curves is that the degree of cooperativity appears to be independent of pH and temperature. In other words, identical saturation curves are obtained over a range of pH and temperature if the concentration scale is chosen (for example) so that half-saturation always occurs at concentration unity. This means in particular that our model parameter $U = 0.55$ is independent of pH and temperature (J, of course, does depend on pH and temperature).

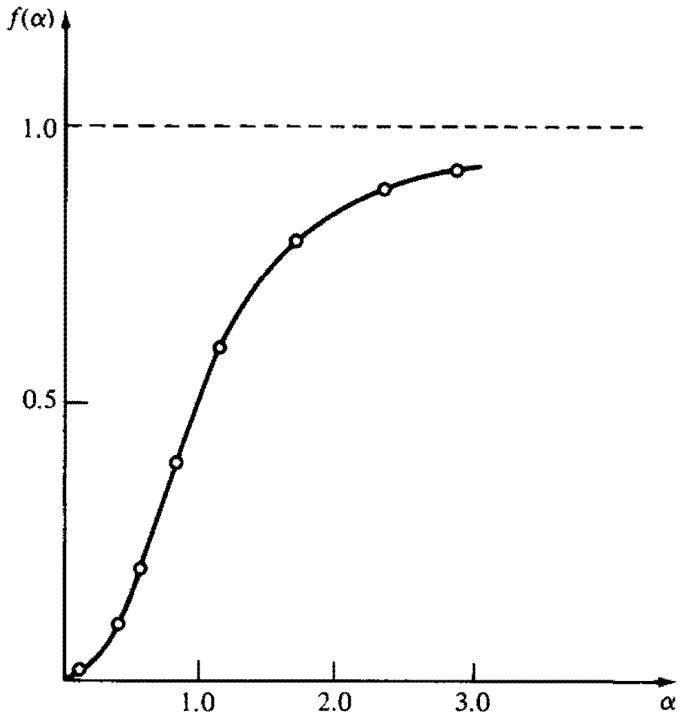

FIGURE 7.5. Fraction of oxygenated hemoglobin $f(\alpha)$ as a function of oxygen concentration α in units such that half-saturation occurs at concentration unity. The solid curve is obtained from Equation 3.11 with $U = 0.55$ and the circles are experimental values taken from Changeux (1965).

7-4 Monod–Wyman–Changeux Model for Hemoglobin and Allosteric Enzymes

Hemoglobin is considered as a prototype for the recently discovered allosteric enzymes, which are characterized by sigmoid-shaped initial reaction-rate (or saturation) curves, rather than by curves of the Michaelis–Henri type for classical enzymes (Figure 7.1). Hemoglobin is, of course, not an enzyme, but it does have an S-shaped saturation curve, and its does have distinct binding sites for "substrate" (i.e., oxygen). Unfortunately, almost nothing is known about the structure of allosteric enzymes except that they have distinct binding sites for substrate.

Typically, allosteric enzymes are also regulatory enzymes. The enzyme aspartate transcarbamylase (ATCase), for example, with aspartate as substrate catalyses a reaction with citosine triphosphate (CTP) as an end product. With CTP present, the initial aspartate reaction is inhibited. In other words, CTP controls or regulates the rate of its own production. Such regulatory or

feed-back behavior appears to be extremely important in body chemistry and is thought to be caused by cooperative interactions (or "allosteric effects") among the binding sites on the enzyme [Changeux (1965)].

A model for such behavior was proposed in 1965 by Monod, Wyman, and Changeux (1965). We shall discuss this (MWC) model here before discussing some generalizations of the Ising model as models for allosteric enzymes in the following section.

The MWC model assumes first of all that the *whole molecule* can exist in one of two conformational states (i.e., states with different "shapes") denoted by R (for relaxed) and T (for tense), respectively, *independently of whether substrate is bound to the enzyme or not*. X-ray data for hemoglobin show that the molecule does undergo conformational changes when oxygen binds to the molecule, but not otherwise; so it would seem that the first assumption in the MWC model is rather unrealistic. The second assumption is that binding in each of the two conformational states is an independent process. That is, there are no interactions or correlations between the binding sites. This also appears to be a little unrealistic in view of our discussion in the previous section.

Let us consider first an enzyme in the presence of substrate only. In the present language the MWC is then very simple. We introduce an additional parameter σ which takes values $+1$ if the molecule is in an R state and -1 if the molecule is in a T state. A configuration is then specified by

$$\{\sigma; \mu\} = (\sigma; \mu_1, \mu_2, \ldots, \mu_n), \tag{4.1}$$

the σ to tell which state the molecule is in and the $\mu_i = \pm 1$, $i = 1, 2, \ldots, n$, as before, to tell which sites are occupied and which sites are unoccupied. Since binding is assumed to occur independently in each state (R or T) the probability distribution is a sum of two independent distributions (Equation 2.8), i.e.,

$$P\{\sigma; \mu\} = Z^{-1}\left[\tfrac{1}{2}(1+\sigma)\prod_{i=1}^{n} e^{J_1(1+\mu_i)} + \frac{L}{2}(1-\sigma)\prod_{i=1}^{n} e^{J_2(1+\mu_i)}\right], \tag{4.2}$$

where for normalization

$$\begin{aligned} Z &= \sum_{\{\sigma;\mu\}}\left[\frac{1}{2}(1+\sigma)\prod_{i=1}^{n} e^{J_1(1+\mu_i)} + \frac{L}{2}(1-\sigma)\prod_{i=1}^{n} e^{J_2(1+\mu_i)}\right] \\ &= \sum_{\{\mu\}}\prod_{i=1}^{n} e^{J_1(1+\mu_i)} + L\sum_{\{\mu\}}\prod_{i=1}^{n} e^{J_2(1+\mu_i)} \\ &= (1+\alpha)^n + L(1+c\alpha)^n. \end{aligned} \tag{4.3}$$

$$\alpha = \exp(2J_1) \tag{4.4}$$

is the ratio of the probability that a site is occupied to the probability that a site is unoccupied in the R state and

$$c\alpha = \exp(2J_2) \tag{4.5}$$

is the ratio of the probability that a site is occupied to the probability that a site is unoccupied in the T state. α, as before, is assumed to be a measure of the concentration of substrate, and L in Equation 4.2 is the "allosteric constant," i.e., the ratio of the probability of the T state to the probability of the R state in the absence of substrate (i.e., all $\mu_i = -1$).

The average number of occupied sites N is easily found to be given by (see Problem 1)

$$\begin{aligned} \frac{N}{n} &= \frac{1}{2n} \sum_{i=1}^{n} \left[\sum_{\{\sigma;\,\mu\}} (1 + \mu_i) P\{\sigma;\,\mu\} \right] \\ &= \frac{\alpha(1+\alpha)^{n-1} + Lc\alpha(1+c\alpha)^{n-1}}{(1+\alpha)^n + L(1+c\alpha)^n}. \end{aligned} \tag{4.6}$$

The similarity in form of Equations 4.6 and 3.8 should be noted.

In the MWC model an S-shaped saturation curve is obtained, for example, by taking L small and c large, which is to say that the number of T molecules is small compared with the number of R molecules, but the probability of binding to a T molecule is large compared with the probability of binding to an R molecule. It is this competitive effect that produces in a somewhat artificial way the characteristic S-shaped saturation curve.

Equation 4.6 fits hemoglobin and allosteric enzyme data rather well [Monod et al. (1965)], which is perhaps not surprising in view of the fact that there are two adjustable parameters (L and c). As we have remarked, the basic assumptions of the model seem to be rather unrealistic since it is likely that there are interactions between binding sites, and that conformational changes of the molecule and binding of substrate to the molecule are not independent of one another. Notice also that the model takes no account of structure. For hemoglobin this is a definite defect in the model, but for allosteric enzymes, where almost nothing is known about structure, it may be an advantage. By considering more sophisticated models, however, it may be possible to deduce some structural information (but probably not a great deal) from the saturation curves. Some work along these lines is discussed in the following section.

In conclusion we remark that the MWC model above can be generalized to take various modifiers (e.g., CTP for ATCase) into account (see Problem 2). These generalized models also fit the experimental data rather well.

7-5 Decorated Ising Models for Allosteric Enzymes

There are 30 or so known allosteric enzymes, but unfortunately almost nothing is known about their structure, even their quaternary structure, i.e., the number of subunits or binding sites. The most studied allosteric enzyme has been aspartate transcarbamylase (ATCase). Early experiments on ATCase [Gerhart and Pardee (1963) and Gerhart and Schachman (1965)] demonstrated that there were separate distinct binding sites for substrate and for modifiers (e.g., the inhibitor CTP). This appears to be still the case. The number of binding sites in each case, however, is a little in doubt at the moment. The original experiments suggested that there were eight binding sites for substrate (catalytic sites) and eight binding sites for modifiers (regulatory sites). More recent experiments by the original group [Changeux and Schachman (1968a), Changeux and Rubin (1968b) and Gerhart and Schachman (1968)] suggest four regulatory and four catalytic sites, whereas an independent group [Weber (1968)] suggests six catalytic sites and six regulatory sites. Let us suppose then that there are $n(4 \leq n \leq 8)$ catalytic sites and $m(4 \leq m \leq 8)$ regulatory sites on the enzyme.

A possible model for ATCase in the absence of modifiers is the model discussed in Section 7-3 with probability distribution given by Equation 3.1 and average number of occupied (catalytic) sites given by Equation 3.8.

For the model to be reasonably close to the truth we need the molecule to have a one-dimensional interaction structure. By this we mean that contacts between subunits can be traced along a one-dimensional path, as for hemoglobin. The molecule will, of course, have a three-dimensional shape, as hemoglobin does, if for no other reason than the molecule will want to occupy the minimum volume.

On general grounds one might argue that all biological molecules have essentially a one-dimensional interaction structure. If this were not so, it would be virtually impossible to make such molecules either naturally or artificially by stringing together components in a definite sequence, which is the way it is done artificially and is probably the way nature does it as well.

If the one-dimensional interaction structure is granted, and if it is assumed

that only nearest-neighbor subunits interact, the probability distribution (3.1) for configurations of the molecule is the only possibility.

The fact that the number of subunits is not known precisely is of little concern, since for the model the fraction of occupied sites given by Equation 3.8 is rather insensitive to n for $n \geq 4$ or so. Thus in Equation 3.8 if we divide top and bottom by $(1 + \alpha + \delta)^n$ and allow n to approach infinity we obtain, since

$$\lim_{n\to\infty} \left(\frac{1 + \alpha - \delta}{1 + \alpha + \delta}\right)^n = 0,$$

$$\lim_{n\to\infty} \frac{N}{n} = \frac{\alpha(\delta + \alpha - 1 + 2e^{-4U})}{\delta(1 + \alpha + \delta)}. \tag{5.1}$$

The error committed in approximating Equation 3.8 by Equation 5.1 for finite n is then exponentially small in n and hence constitutes a negligible error for n larger than about 4.

In Figure 7.6 we have compared a theoretical curve obtained from Equation 3.8 with $n = 8$, with experimental values obtained for ATCase in the

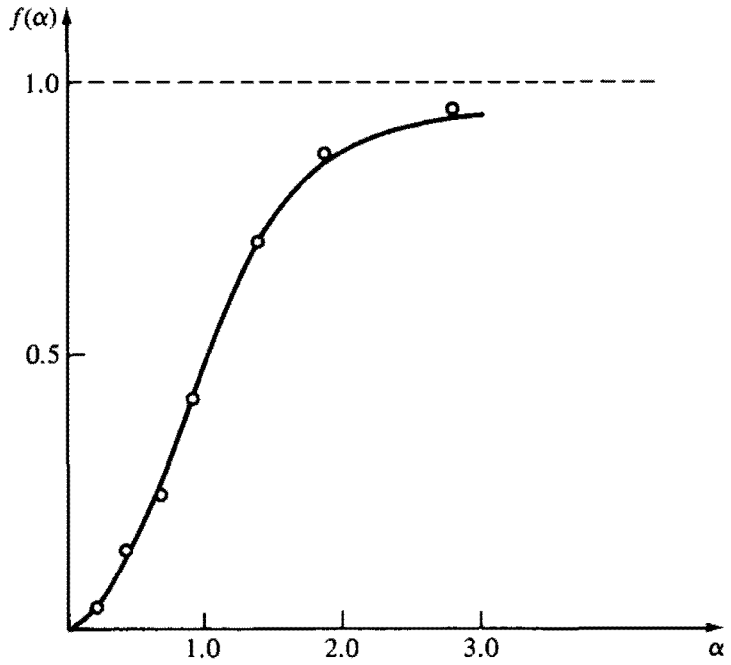

FIGURE 7.6. Saturation curve for ATCase in the absence of modifiers. The solid curve is obtained from Equation 3.8 with $n = 8$ and $U = 0.55$ and the circles are experimental values taken from Gerhart and Pardee (1963).

presence of substrate only [Gerhart and Pardee (1963)]. The value of U that best fits the data is 0.55, which is surprisingly the same value obtained for hemoglobin.

We consider now a modification of the model 3.1 to take occupation of regulatory sites into account.

In the presence of CTP, as we have noted, the initial reaction rate is inhibited as shown in Figure 7.7; i.e., the saturation curve moves off to the right in the presence of CTP, making the initial reaction rate smaller for a fixed substrate concentration in the presence of CTP.

The precise number m of regularity sites is unfortunately not known ($4 \leq m \leq 8$) and the arrangement of the regulatory subunits with respect to the catalytic subunits is also not known. We consider here only one possible

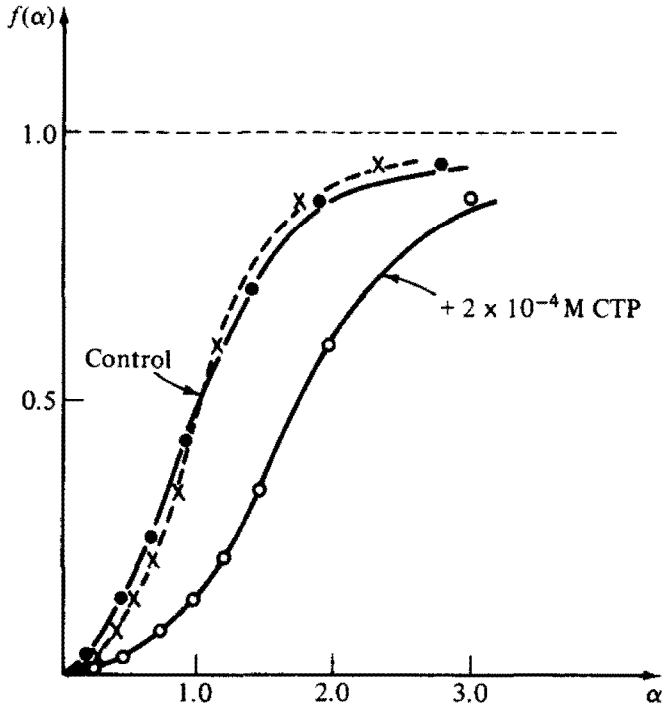

FIGURE 7.7. Saturation curves for ATCase. Black circles are experimental values for control (no CTP) and white circles are experimental values for ATCase in the presence of 2×10^{-4} M CTP. The solid curve for control is obtained from Equation 3.8 with $n = 8$ and $\exp(-4U) = 0.11$; the solid CTP curve is obtained from Equation 3.8 with α and U replaced by $\bar{\alpha}$ and $\bar{U}$ (Equations 5.9 and 5.10) and $n = 8$ and $\exp(-4\bar{U}) = 0.10$. The dashed curve is the CTP curve rescaled so that half-saturation occurs at concentration unity. The crosses are the rescaled experimental values.

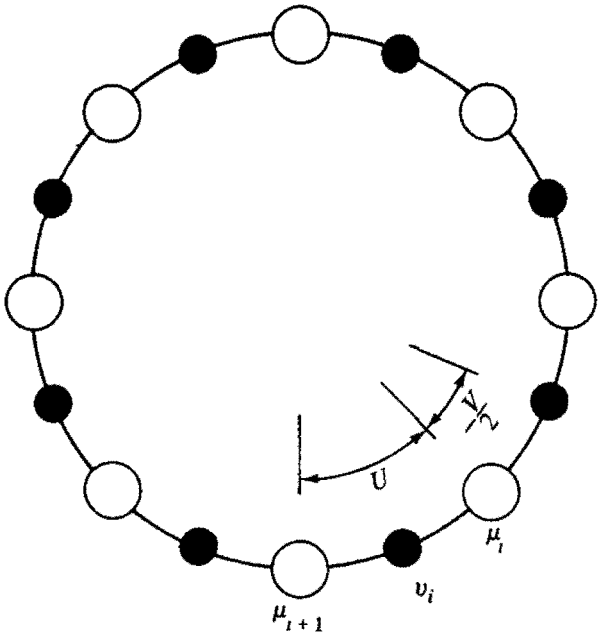

FIGURE 7.8. ATCase model. The white subunits bind substrate and the black subunits bind modifiers (CTP). Neighboring white subunits and neighboring black and white subunits only are assumed to interact.

model, based on the original experiments, which assumes eight catalytic and eight regulatory subunits, as shown in Figure 7.8. As discussed above, assuming four, six, or eight of each will not make any appreciable difference to the saturation curves (the error in any case is probably significantly less than the experimental error).

To take account of CTP in the model shown in Figure 7.8 we introduce a set of additional parameters v_i, $i = 1, 2, \ldots, n$ with values $+1$ if the ith regulatory site [between the ith and $(i+1)$th catalytic sites] is occupied by CTP and -1 if the ith regulatory site is unoccupied by CTP. The parameters μ_i, $i = 1, 2, \ldots, n$, as before, specify the states of the catalytic sites and a configuration of the molecule is specified in the presence of CTP by

$$\{\mu; \nu\} = (\mu_1, \mu_2, \ldots, \mu_n; \nu_1, \nu_2, \ldots, \nu_n). \tag{5.2}$$

We take the probability distribution for such a configuration to be

$$P\{\mu; \nu\} = Z^{-1} \prod_{i=1}^{n} (e^{J\mu_i} e^{U\mu_i\mu_{i+1}})[e^{I(1+\nu_i)} e^{-V/4(1+\nu_i)(\mu_i+\mu_{i+1})}], \tag{5.3}$$

where for normalization

$$Z = \sum_{\{\mu;\,\nu\}} \prod_{i=1}^{n} (e^{J\mu_i} e^{U\mu_i\mu_{i+1}})[e^{I(1+\nu_i)} e^{-V/4(1+\nu_i)(\mu_i+\mu_{i+1})}]. \tag{5.4}$$

When all $v_i = -1$, i.e., all regulatory sites are unoccupied, Equation 5.3 reduces, as it should, to the previous model Equation 3.1. The factor $\exp[I(v_i + 1)]$ in Equation 5.3 represents independent binding on the regulatory sites and the last factor, $\exp[-(V/4)(1 + v_i)(\mu_i + \mu_{i+1})]$ with $V > 0$, represents repulsive interactions between nearest-neighbor regulatory and catalytic sites. We have not included any interactions between neighboring regulatory sites since it is found experimentally that ATCase, in the presence of CTP only, fits the classical Michaelis–Henri equation; i.e., there are no apparent interactions among regulatory sites.

Note that the "interaction term" in Equation 5.3,

$$U\mu_i\mu_{i+1} - \frac{V}{4}(1 + v_i)(\mu_i + \mu_{i+1}) = U - V \tag{5.5}$$

when $\mu_i = \mu_{i+1} = v_i = +1$, i.e., when the ith regulatory site and its two neighboring catalytic sites *are all occupied.* This means that when $U = V$, which, in fact, turns out to be the choice that best fits the data, the repulsive interaction between *occupied* neighboring regulatory and catalytic sites, completely annihilates the attractive interaction between *occupied* neighboring catalytic sites. In other words, $U = V$ for the present model corresponds to complete inhibition.

The evaluation of Z (Equation 5.4), which in magnetic language is the partition function for a "decorated Ising model" (or an Ising magnet with spin impurities), is accomplished in much the same way as before with the aid of the transfer-matrix method. Thus, if we first sum over the v variables in Equation 5.4 we obtain

$$Z = \sum_{\{\mu\}} \prod_{i=1}^{n} L'(\mu_i, \mu_{i+1}), \tag{5.6}$$

where

$$L'(\mu_i, \mu_{i+1}) = e^{J\mu_i/2} e^{U\mu_i\mu_{i+1}}[1 + e^{2I} e^{-V/2(\mu_i + \mu_{i+1})}] e^{J\mu_{i+1}/2},$$

or, in matrix form,

$$\mathbf{L}' = \begin{array}{c} \\ \mu_i = +1 \\ \mu_i = -1 \end{array} \begin{array}{c} \begin{array}{cc} \mu_{i+1} = +1 & \mu_{i+1} = -1 \end{array} \\ \begin{pmatrix} e^{U+J}(1 + \beta e^{-V}) & e^{-U}(1 + \beta) \\ e^{-U}(1 + \beta) & e^{U-J}(1 + \beta e^{V}) \end{pmatrix} \end{array}$$

$$= (1 + \beta) e^{U-U} \begin{pmatrix} e^{U+J} & e^{-U} \\ e^{-U} & e^{U-J} \end{pmatrix}, \tag{5.7}$$

where

$$\beta = e^{2I} \tag{5.8}$$

is a measure of the CTP concentration, $\alpha = e^{2J}$ (as before) is a measure of the substrate concentration, and $\bar{U}$ and $\bar{J}$ are defined by

$$\begin{aligned}\bar{\alpha} &= e^{2\bar{J}} \\ &= \alpha \frac{1 + \beta e^{-V}}{1 + \beta e^{V}}\end{aligned} \tag{5.9}$$

and

$$e^{4\bar{U}} = e^{4U}\left[1 + \frac{4\beta}{(1+\beta)^2}\sinh^2\left(\frac{V}{2}\right)\right]. \tag{5.10}$$

Apart from the factor $C = (1 + \beta)\exp(\bar{U} - U)$, which is *independent of the substrate concentration* α, the matrix $\mathbf{L}'$ is identical with the matrix $\mathbf{L}$ (Equation 3.5) with J and U replaced by $\bar{J}$ and $\bar{U}$, respectively. It follows that the (two) eigenvalues of $\mathbf{L}'$ are, apart from the constant C, given by Equation 3.6 with J and U replaced by $\bar{J}$ and $\bar{U}$, respectively. The argument leading to Equation 3.7 for the average number of occupied catalytic sites can now be repeated. Since C is independent of J it cancels in Equation 3.7 and we find that the fraction of occupied catalytic sites $f(\alpha)$ is given by Equation 3.8 with α and U replaced by $\bar{\alpha}$ and $\bar{U}$ defined by Equations 5.9 and 5.10, respectively.

Half-saturation occurs when $\bar{\alpha} = 1$ [since $f(1) = \frac{1}{2}$], i.e., from Equation 5.9, when

$$\alpha = \alpha_{1/2} = \frac{1 + \beta e^{V}}{1 + \beta e^{-V}}. \tag{5.11}$$

Since V is assumed to be positive, $\alpha_{1/2}$ is an increasing function of CTP concentration β with the limiting value

$$\lim_{\beta \to \infty} \alpha_{1/2} = e^{2V}. \tag{5.12}$$

The increase of $\alpha_{1/2}$ with increasing CTP concentration is observed experimentally [Figure 7.7, Gerhart and Pardee (1963)] and so is the limiting behavior described by Equation 5.12. Notice that in our model the limiting value of $\alpha_{1/2}$ is directly related to the interaction parameter V between regulatory and catalytic sites.

It is clear from Equation 5.10 that $\bar{U} \geq U$; i.e., in the presence of CTP the "effective interaction" between catalytic sites is increased. Notice, however, from Equation 5.10, that $\bar{U}$ as a function of β achieves a maximum value $\bar{U}_M$ given by

$$e^{4\bar{U}_M} = e^{4U}\left[1 + \sinh^2\left(\frac{V}{2}\right)\right] \tag{5.13}$$

when $\beta = 1$, and that $\lim_{\beta \to \infty} \bar{U} = U$. In other words, according to the model, cooperativity should at first increase with increasing CTP concentration until it reaches a maximum at a certain concentration $\beta_M (= 1$ in our units), and for $\beta > \beta_M$ cooperativity should decrease until in the limit $\beta \to \infty$, $\bar{U} = U$, which is also the case when $\beta = 0$. This effect should be clearly visible if the saturation curves for different CTP concentrations are plotted on a scale so that half-saturation always occurs at concentration unity (see Figure 7.7). Unfortunately, the data necessary to test this prediction do not seem to exist. The only published data for ATCase of the desired type [Gerhart and Pardee (1963)] give two saturation curves (shown in Figure 7.7), one for ATCase in the absence of modifiers ("control") and one in the presence of 2×10^{-4} M CTP. These two curves are sufficient, however, to determine all the parameters in the model (U, V, and the scale of concentration β).

With the control $\alpha_{1/2} = 1$ we have found that the choice $U = 0.55$ best fits the control data. In the presence of 2×10^{-4} M CTP, $\alpha_{1/2} \cong 1.7$ (from Figure 7.7), so from Equation 5.11 we obtain

$$\frac{1 + \beta e^{V}}{1 + \beta e^{-V}} \cong 1.7. \tag{5.14}$$

Furthermore, if we rescale the CTP curve as described above (shown as a dashed curve in Figure 7.7) and fit the resulting curve to Equation 3.8 we obtain $\exp(-4\bar{U}) \cong 0.10$. Since $\exp(-4U) \cong 0.11$ we find from Equation 5.10 that

$$\frac{4\beta}{(1 + \beta)^2} \sinh^2\left(\frac{V}{2}\right) \cong 0.10. \tag{5.15}$$

Solving Equations 5.14 and 5.15 for β and V we obtain

$$\beta \cong 0.93 \tag{5.16}$$

and

$$\exp(2V) \cong 3.0. \tag{5.17}$$

The values of β and V are unfortunately very sensitive to the values of $\bar{U}$ and U, so Equations 5.16 and 5.17 could conceivably be in error by as much as 20 percent or so (if $\bar{U}$ and U are in error by a few percent).

Nevertheless, from Equations 5.17 and 5.12 we conclude that the ratio of $\alpha_{1/2}$ in the limit of infinite CTP concentration, to $\alpha_{1/2}$ for no CTP, should be approximately 3. Also, from Equation 5.16 and the above discussion, we conclude that maximum cooperativity should be achieved at a CTP concentration of about 2×10^{-4} M. Unfortunately, the data to test either of these predictions do not seem to exist.

One interesting result, which emerges from Equation 5.17, is that $V \approx U \approx 0.55$, which means, as remarked above, that in the model, at least, we have complete inhibition.

The model described above can be generalized in any number of ways, for example, to take activators, which shift the curve to the left, as well as inhibitors into account on ATCase. Models can also be formulated for allosteric enzymes that do not have distinct subunits for substrate and modifiers (e.g., DPN–isocitrate dehydrogenase). Some discussion of these cases can be found in Thompson (1968b) (see Problem 3).

7-6 Ising Models for DNA

Deoxyribonucleic acid (DNA for short) is the blueprint for life, the carrier of the genetic code. Naturally occurring DNA is a large molecule, typically 30,000 Å long and 20 Å thick, composed of some 1 million atoms. It contains four essential components, called bases: adenine (A), thymine (T), cytosine (C), and guanine (G); and sections of the molecule from a given organism, consisting of sequences of A's, T's, C's, and G's, are claimed to determine the set of proteins that the organism can make.

According to the Watson–Crick model [Watson (B1968)] DNA is composed of two strands wrapped around one another to form a double helix, as shown in Figure 7.9. There are sequences of the four bases on each strand which are connected to one another by (relatively weak) hydrogen bonds, also shown in Figure 7.9. An important feature of the model is that A can only be coupled to T, and C can only be coupled to G, so AT and CG are the only possible base pairs. In the model this is necessary to obtain a compact structure. The occurrence of equal amounts of A and T and of C and G was,

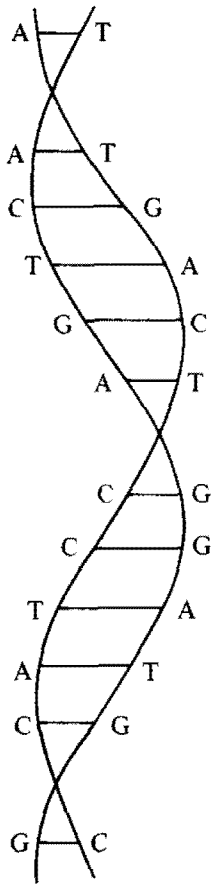

FIGURE 7.9. Watson–Crick model for DNA.

however, discovered by Chargaff (1950) before the invention of the Watson–Crick model and is known as Chargaff's rule.

Because of Chargaff's rule and the two-stranded structure, the sequence of bases on one strand completely determines the complementary sequence of bases on the other strand. This has very important genetic implications. Replication of DNA, for example, can be achieved in the model by unwinding the molecule and making two new complementary strands from free bases. The sequence of bases on one strand (or its complementary sequence) is also claimed to be the blueprint for the production of proteins.

Since the model is so simple and explains almost everything that needs to be explained, it has been almost universally accepted. Its inventors, Crick and Watson, and also Wilkins, who provided the X-ray pictures that suggested a double-helix structure, were justly rewarded with the Nobel prize for medicine in 1962—the same year, in fact, that Perutz and Kendrew were awarded the chemistry prize for the structure of hemoglobin and myoglobin. Some very

recent work, however, suggests that the structure of DNA may not be quite as simple as that proposed by Watson and Crick. Wu (1969), in particular, has made a very careful reevaluation of the X-ray pictures (at high humidity) and finds that the data fit a four-strand model much better than a two-strand model. The final word on the subject, however, will have to wait until more detailed X-ray pictures become available.

The considerable amount of theoretical work that has been done on the Watson–Crick model has been mainly concerned with the denaturation process, i.e., the breaking of the hydrogen bonds connecting the two strands under treatment by heat or other things, such as pH. As the temperature is increased, for example, bonds break until finally one is left with two separate strands or coils. The denaturation process, or helix-coil transition, produces melting curves (the fraction of broken bonds as a function of temperature) with the characteristic sigmoid shape shown in Figure 7.10, reflecting some degree of cooperativity or interaction among the hydrogen bonds connecting the two strands. The temperature T_1 where one half of the bonds are broken is called the melting point, and around this point the bonds break rather easily.

The first theoretical treatment of the denaturation process was given by

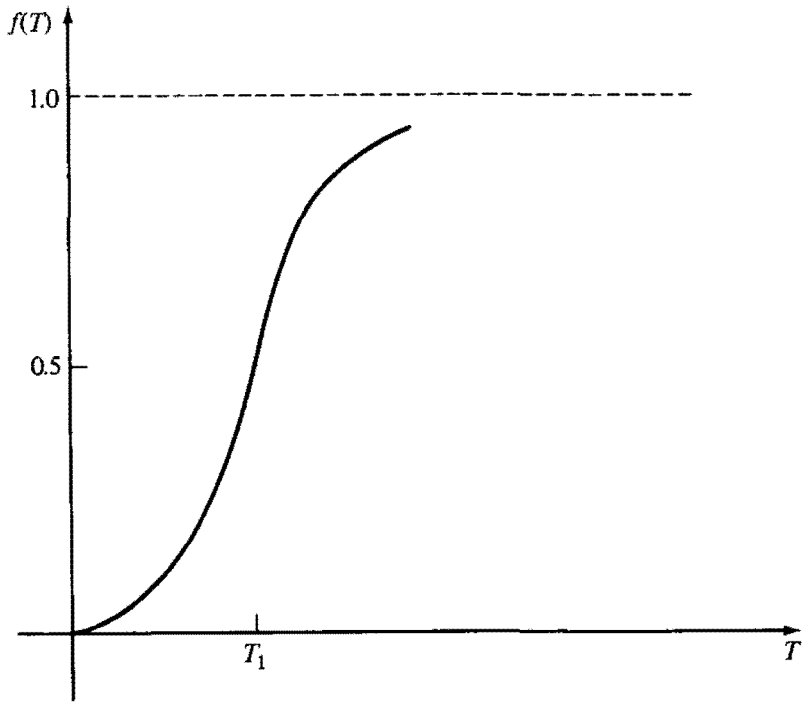

FIGURE 7.10. Fraction of broken bonds $f(T)$ as a function of temperature T. One half of the bonds are broken at the melting point T_1.

Zimm and Bragg (1959), who assumed that all bonds are identical. This is surely not the case in naturally occurring DNA, since AT pairs are connected by two hydrogen bonds, while CG pairs are connected by three hydrogen bonds. Synthetic one-component DNA's consisting of all AT or all CG pairs can be made, however, and the Zimm–Bragg model should be applicable to such molecules. We begin, therefore, with a discussion of one-component DNA. The presentation given by Montroll and Goel (1966) and Goel and Montroll (1968) will be followed throughout, since they use Ising-model language exclusively. Various periodic synthetic two-component (i.e., AT and CG pairs) DNA molecules are also discussed by Montroll and Goel, and we shall have a little to say about these at the end of this section. The interested reader is referred to Montroll and Goel (1966) and Goel and Montroll (1968) for lists of references and relations between previous work and the models to be discussed here.

For all intents and purposes we can consider the Watson–Crick model as the ladder shown in Figure 7.11, the sides of the ladder corresponding to the two strands and the rungs of the ladder to the complexes joining the base pairs. By complexes we mean the two hydrogen bonds connecting an AT

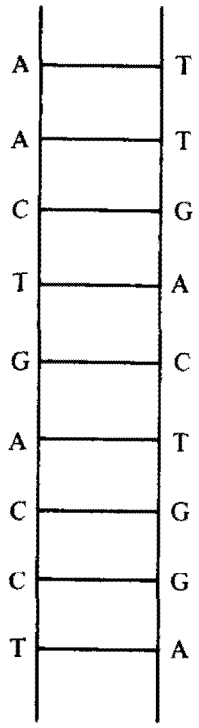

FIGURE 7.11. Ladder version of the Watson–Crick model (Figure 7.9).

pair and the three hydrogen bonds connecting a CG pair. We number the complexes by an index $i = 1, 2, \ldots, n$ and assume for simplicity that a complex is either broken or intact. We then assign a parameter μ_i to the ith complex with values

$$\mu_i = \begin{cases} +1 & \text{if the } i\text{th complex is broken} \\ -1 & \text{if the } i\text{th complex is intact.} \end{cases} \tag{6.1}$$

In a given configuration of broken and intact complexes $\{\mu\} = (\mu_1, \ldots, \mu_n)$, the number of broken complexes is given by

$$N\{\mu\} = \sum_{i=1}^{n} \tfrac{1}{2}(1 + \mu_i), \tag{6.2}$$

and if $P\{\mu\}$ is the probability distribution for the configuration $\{\mu\}$, the average number of broken complexes N is given by

$$N = \sum_{\{\mu\}} N\{\mu\}P\{\mu\}, \tag{6.3}$$

where the sum is over all (2^n) possible configurations $\mu_1 = \pm 1$, $\mu_2 = \pm 1, \ldots,$ $\mu_n = \pm 1$ of the molecule.

The formulation given so far is completely general and is equivalent to the formulation given in previous sections for hemoglobin and (allosteric) enzymes. The problem, as before, is to specify the probability distribution $P\{\mu\}$.

Consider first the random one-component case, i.e., with probability distribution $P\{\mu\}$ given by Equations 2.7 and 2.8,

$$P\{\mu\} = \prod_{i=1}^{n} p(\mu_i), \tag{6.4}$$

$$p(\mu_i) = (2 \cosh J)^{-1} \exp(J\mu_i), \tag{6.5}$$

where now $p(+1)$ is the probability that a complex is broken and $p(-1)$ is the probability that a complex is intact. In this case the fraction of broken complexes f is given by Equation 2.12, i.e.,

$$\begin{aligned} f &= \frac{N}{n} \\ &= \tfrac{1}{2}(1 + \tanh J). \end{aligned} \tag{6.6}$$

To determine the temperature dependence of f we must determine the temperature dependence of J. The obvious statistical-mechanical choice, from Equation 6.5, is $J = E/kT$, where E is the energy difference between bonded and unbonded states. In the limit of infinite temperature ($J = 0$), however, Equation 6.6 then gives $f = \frac{1}{2}$, which is certainly incorrect since we know from experiment that all bonds are broken at sufficiently high temperatures. E, defined above, must then be temperature dependent if we wish to imitate Figure 7.10 with Equation 6.6. We therefore make the empirical choice

$$J = a(T - T_1). \tag{6.7}$$

$f = f(T)$ is then one half at the melting point T_1 and Equation 6.6 gives the curve shown in Figure 7.12.

The slope of the curve at $T = T_1$ from Equations 6.6 and 6.7 is obviously $a/2$, so the melting curve can be made more "cooperative" or less "cooperative" by increasing or decreasing a.

For pure synthetic AT-DNA, Equations 6.6 and 6.7 give a reasonably good fit to experiment with the choice $a = 1$ and $T_1 = 65°C$.

The random model, however, is a little unrealistic and does not in general give a good fit to experiment. A more reasonable choice for the probability

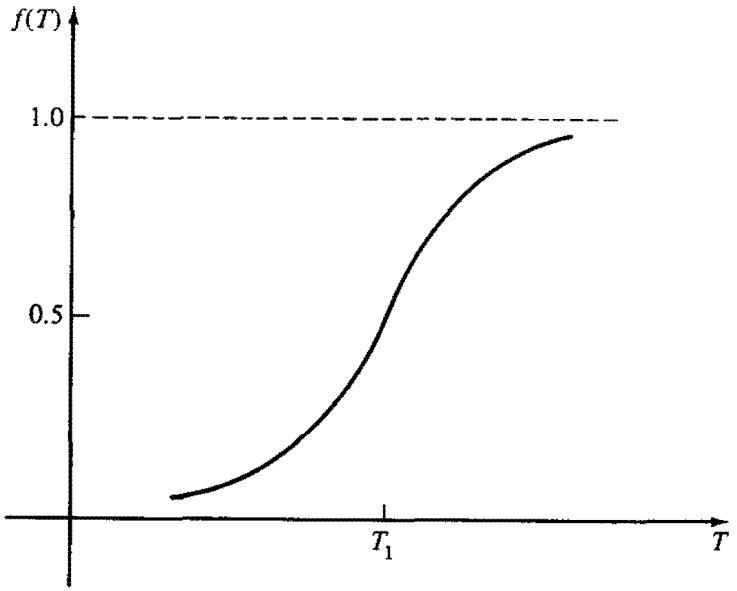

FIGURE 7.12. Melting curve obtained from the random model Equations 6.6 and 6.7.

distribution $P\{\mu\}$, which takes nearest-neighbor complex interactions into account, is (Equation 3.1)

$$P\{\mu\} = Z^{-1} \prod_{i=1}^{n} e^{J\mu_i} e^{U\mu_i\mu_{i+1}}, \tag{6.8}$$

where

$$Z = \sum_{\{\mu\}} \prod_{i=1}^{n} e^{J\mu_i} e^{U\mu_i\mu_{i+1}} \tag{6.9}$$

is again the Ising-model partition function, and for simplicity we have taken $\mu_{n+1} = \mu_1$, i.e., "circular DNA" (since n is large, boundary, or free end, terms are unimportant).

The fraction of broken complexes from Equations 3.6 and 3.7 is given by

$$f = \frac{N}{n} = \frac{1}{2}\left[1 + (\lambda_1^n + \lambda_2^n)^{-1}\left(\lambda_1^{n-1}\frac{\partial\lambda_1}{\partial J} + \lambda_2^{n-1}\frac{\partial\lambda_2}{\partial J}\right)\right], \tag{6.10}$$

where

$$\left.\begin{matrix}\lambda_1\\ \lambda_2\end{matrix}\right\} = e^U \cosh J \pm (e^{-2U} + e^{2U}\sinh^2 J)^{1/2}. \tag{6.11}$$

In the limit $n \to \infty$ only the largest eigenvalue λ_1 contributes to Equation 6.10, giving

$$f = \lim_{n\to\infty}\frac{N}{n} = \frac{1}{2}\left[1 + \frac{\sinh J}{(e^{-4U} + \sinh^2 J)^{1/2}}\right]. \tag{6.12}$$

In the limit $U = 0$ (i.e., no interactions) Equation 6.12 reduces to the random model equation (6.6) and in the limit $U \to \infty$, the "zipper limit," f becomes a step function; i.e., $f = 1$ when $J > 0$ and $f = 0$ when $J < 0$, as shown in Figure 7.13 for the choice $J = a(T - T_1)$ (Equation 6.7).

In general the model gives a reasonably good fit to experiment, but it has one serious deficiency—it does not take long sequences of broken bonds into account in a realistic way. As bonds break, rings or loops are formed by the separated strands. Such rings can exist in a number of possible geometrical configurations, giving rise, in statistical-mechanical language, to a ring entropy. Also it is reasonable to suppose that bonds will break more easily in the neighborhood of a loop. Neither of these effects is taken into account in Equation 6.8 for the probability distribution $P\{\mu\}$.

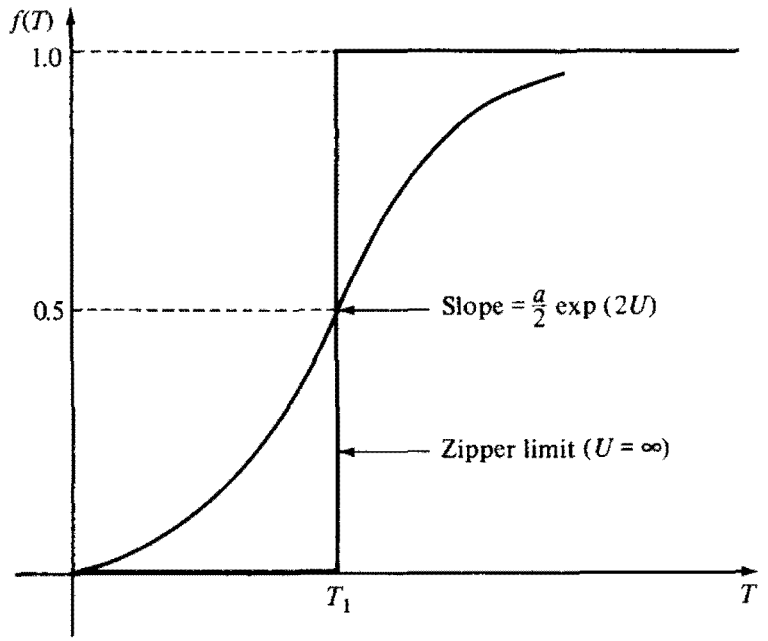

FIGURE 7.13. Melting curves obtained from Equation 6.12.

Various models have been proposed to take account of the ring entropy [see Goel and Montroll (1968) and references therein], but none is entirely satisfactory. It should be noted, however, that the above model is probably a reasonably good model for temperatures below the melting point, where large rings or loops are not yet formed.

The Ising model can in principle be modified to take loops and different complexes (AT and CG) into account, but the mathematical manipulation required then becomes extremely unwieldy. One interesting question, which has not been satisfactorily answered, is: Can one deduce any (statistical) information about the distribution of base pairs in naturally occurring DNA from the melting curves? In an attempt to answer this question Goel and Montroll considered various synthetic DNA's with known periodic distribution of AT's and CG's. One obtains a variety of melting curves for such molecules (some examples are shown in Figure 7.14) and the hope is that by considering simple models for such molecules, model parameters will be found to fit more complicated DNA forms.

One interesting fact that appears to emerge from these studies is that the coupling constant U is temperature independent and is essentially the same for nearest-neighbor AT-AT, AT-GC, or GC-GC complexes. Assuming that U is, in fact, independent of temperature and complex, a probability dis-

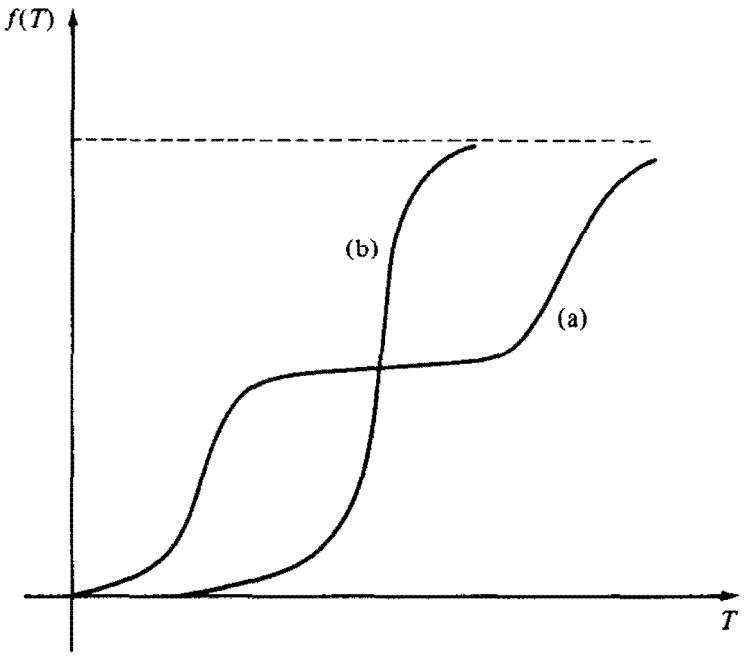

FIGURE 7.14. Melting curves for DNA:

(a) A A A ··· A G G G
| | | | | | |
T T T T C C C

(b) A G A G
| | | | ···
T C T C

tribution $P\{\mu\}$ appropriate for the sequence of AT's and CG's shown in Figure 7.15 is

$$P\{\mu\} = Z^{-1}\left(\prod_{i=1}^{n} e^{U\mu_i\mu_{i+1}}\right)e^{J_1(\mu_1+\cdots+\mu_l)}e^{J_2(\mu_{l+1}+\cdots+\mu_{l+m})} \times e^{J_1(\mu_{l+m+1}+\cdots+\mu_{l+m+s})}\cdots, \tag{6.13}$$

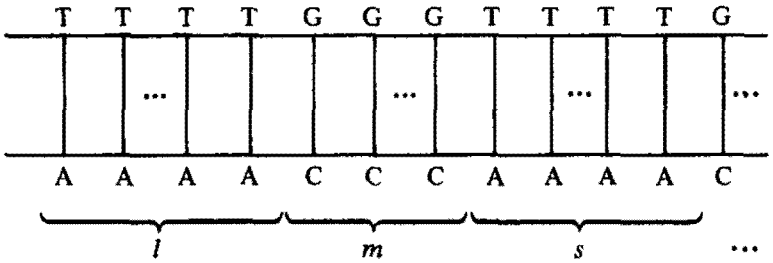

FIGURE 7.15. Periodic two-component DNA.

where J_1 refers to AT complexes and J_2 to CG complexes. The evaluation of the fraction of broken bonds for such a distribution can be carried out with the aid of transfer-matrix methods (see Problem 4 for some special cases) and, if one wishes, loops can be included as well.

PROBLEMS

1. Derive Equation 4.6 for the fraction of occupied sites in the Monod–Wyman–Changeux model.

2. Construct a probability distribution for the following generalized Monod–Wyman–Changeux model:

(a) The whole molecule can exist in either an R state or a T state;

(b) Substrate (S) binds exclusively to molecules in the R state;

(c) Inhibitor (I) binds exclusively to molecules in the T state;

(d) Activator (A) binds exclusively to molecules in the R state. Assuming that there are n binding sites for S, I, and A, show that the fraction of sites occupied by substrate is given by

$$\frac{\alpha(1+\alpha)^{n-1}(1+\gamma)^n}{(1+\alpha)^n(1+\gamma)^n + L(1+\beta)^n},$$

where L is the allosteric constant (Equation 4.2) and α, β, and γ are the concentrations of substrate, inhibitor, and activator, respectively.

3. Consider a molecule composed of n subunits with one binding site for substrate and one binding site for inhibitor on each subunit. Assuming that only nearest-neighbor substrate sites interact and that occupation of a subunit by inhibitor affects only the substrate occupation of that subunit, show that the probability distribution given by (see Equation 5.3)

$$P\{\mu; \nu\} = Z^{-1} \prod_{i=1}^{n} \exp\left[J\mu_i + U\mu_i\mu_{i+1} + I(1+\nu_i) - \frac{V}{2}(1+\nu_i)\mu_i\right]$$

leads to the fraction of occupied substrate sites $f(\bar{\alpha})$ given by Equation 3.8 with $\bar{\alpha}$ defined by Equation 5.9 (and U unchanged). (This is a possible model for DPN–isocitrate dehydrogenase [Thompson (1968b)].)

4. The probability distribution for periodic AT, CG, AT, CG, ... DNA, excluding loop effects and assuming only nearest-neighbor complex interactions, is given by (Equation 6.13)

$$P\{\mu\} = Z^{-1}\left(\prod_{i=1}^{2n} e^{U\mu_i\mu_{i+1}}\right) e^{J_1(\mu_1+\mu_3+\cdots+\mu_{2n-1})}\, e^{J_2(\mu_2+\mu_4+\cdots+\mu_{2n})},$$

where J_1 refers to AT complexes and J_2 to CG complexes. Use the transfer-matrix method to calculate the average number of broken bonds, assuming that $J_1 = a(T - T_1)$ and $J_2 = a(T - T_2)$.

Do the same for AT-AT-AT $\cdots$ AT-CG-CG $\cdots$ CG DNA, assuming only one interaction parameter U for nearest-neighbor complexes.